CORA Cork Open Research Archive
Cartlann Taighde Oscailte Chorcaí

Title	Multiple proton diffusion and film densification in atomic layer deposition modeled by density functional theory
Authors	Shirazi, Mahdi;Elliott, Simon D.
Publication date	2013-02-28
Original Citation	SHIRAZI, M. & ELLIOTT, S. D. 2013. Multiple Proton Diffusion and Film Densification in Atomic Layer Deposition Modeled by Density Functional Theory. Chemistry of Materials, 25, 878-889. http://dx.doi.org/10.1021/cm303630e
Type of publication	Article (peer-reviewed)
Link to publisher's version	10.1021/cm303630e
Rights	© 2013 American Chemical Society. This document is the Accepted Manuscript version of a Published Work that appeared in final form in Chemistry of Materials, copyright © American Chemical Society after peer review and technical editing by the publisher. To access the final edited and published work see http://dx.doi.org/10.1021/cm303630e
Download date	2026-11-13 01:37:29
Item downloaded from	https://hdl.handle.net/10468/2422



UCC
University College Cork, Ireland
Coláiste na hOllscoile Corcaigh

Multiple proton diffusion and film densification in atomic layer deposition modelled by density functional theory

Mahdi Shirazi* and Simon D. Elliott

Tyndall National Institute, University College Cork, Lee Maltings, Cork, Ireland

E-mail: mahdi.shirazi@tyndall.ie

Abstract

To investigate the atomic layer deposition (ALD) reactions for growth of HfO_2 from $Hf(NMe_2)_4$ (TDMAHf) and H_2O, a density functional theory (DFT) slab model was employed. We inspected all energy steps, from the early stage of adsorption of each ALD precursor to the densification of multiple atoms into bulk-like HfO_2 layers. The activation energy calculations show that repeated proton diffusion from the surface to amide ligands and rotation of the protonated amine is more energetically accessible than the simple elimination of the amine in the initial stage. We therefore propose that multiple protons diffuse to the amide ligands of the Hf precursor before desorption of protonated ligands takes place. Loss of a proton from surface oxygen frees it up for bonding to Hf of the precursor. Protonation of ligands, and especially desorption of ligands, frees up Hf for bonding to surface oxygen. These effects are termed 'densification', as they bring $Hf-O$ packing closer to the bulk scenario. Densification is associated with substantial release of energy. During the metal pulse, saturation of the surface by remaining fragments HfX causes adsorption of further metal precursor to stop. The presence

*To whom correspondence should be addressed

of these fragments prevents further chemisorption of HfX_4, since this requires the creation of a strong dative bond between Hf and O. Next, during the H_2O pulse, Hf exchanges its remaining ligands with OH groups. The exchange occurs due to the decomposition of adsorbed H_2O molecules in clusters of HfX. Decomposition of H_2O when adsorbed onto a $(Hf(NMe_2))_x$ ($x \geq 2$) cluster (e.g. dimers) also increases the coordination of Hf and O. Simultaneously, low-coordinated oxygen atoms appear at the surface, which are reactive sites for the next metal pulse. With saturation of the surface by OH groups, H_2O molecules begin to appear. This detailed description of ALD chemistry allows us to make qualitative predictions about how the process depends on temperature. The data can also be inputted into kinetic simulations for a quantitative view of the complex film growth process.

Introduction

Hafnium oxide (HfO_2) shows a band gap of approximately 6 eV and a high dielectric constant in thin film form of 25 which makes it an important high-*k* material. In the ongoing miniaturization of electronic devices, nanometre-thin films of hafnium oxide are replacing silicon oxide as the gate insulator in field effect transistors.[1] The hafnium oxide thin films are fabricated using atomic layer deposition (ALD).[2] This study unveils the atomic scale reactions of ALD for hafnium oxide thin films.

In ALD, gaseous precursors are allowed individually into the reactor chamber in alternating pulses. The precursors are highly reactive to each other, and so between each pulse inert gas is admitted to prevent gas phase reactions. Each precursor thus chemisorbs onto the substrate, rather than reacting in the gas-phase. In the ideal ALD situation, substrate-precursor reactions are self-controlled. This means that, when the substrate is covered with fragments of precursor at the end of each pulse, other precursors in the gas phase are not able to react with the surface any more. Growth is therefore stopped until the other precursor is admitted in the next pulse and reacts with the remaining fragments. The sequences of pulses and purges is followed until the desired thickness of thin film is obtained.

In ALD of hafnium oxide, $HfCl_4$ and water are the most frequently used precursor combination.[3] However, a major difficulty with the $HfCl_4$ precursor is chlorine contamination in the thin films. The contamination decreases with increasing substrate temperature. However higher temperature means a drop in coverage of reactive OH fragments as H_2O dissociates and consequently a drop in growth rate per cycle. Therefore an alternative precursor chemistry is required that exhibits suitable thermal stability, conformal ALD growth and low levels of impurities at low temperature. Hafnium alkylamide precursors, like $Hf(NEtMe)_4$, $Hf(NEt_2)_4$ and $Hf(NMe_2)_4$ ($Et = C_2H_5$, $Me = CH_3$), are interesting alternatives together with water leading to smooth and conformal thin films.[4] These precursors operate at relatively low temperature ($\sim 300\ ^\circ C$). While there is discussion about the stability of alkylamide precursors as a function of temperature, this is out of the scope of this paper, where we consider only "ideal" ALD reactions. For such ideal reactions, we expect that the three commonly-used amides listed above will behave similarly, and so carry out calculations on just one of them, $Hf(NMe_2)_4$.

The growth of hafnium oxide from $HfCl_4$ and water on different substrates was studied theoretically before.[5,6] The effect of under-coordinated surface oxygen and hydroxyl groups (as the active sites) on the hafnium of adsorbing precursor was inspected and it was shown that the dissociation of HCl is facilitated via increasing the c.n of hafnium during the water pulse.[7] The ALD reactions for elimination of HCl from $HfCl_4$ are computed to be endothermic[5,7] which is in sharp contrast to the success of this precursor in ALD experiments. In the cluster model the neglect of under-coordinated atoms[6] might cause this discrepancy, while in the slab model the neglected change in entropy[7] might be the cause. Therefore, in the current study of metal alkylamide precursors, we consider both the change in entropy and the influence of under-coordinated atoms and find exothermic reactions, which resolves the discrepancy between experiment and theory. Here we should emphasize that some aspect of the reaction pathways for amides are different from those of halides. The amide is more bulky and more reactive toward a hydroxylated surface than the chloride. The amide ligands are more Brønsted basic than chloride ligands. The films deposited by metal alkylamide precursors show a high degree of conformality and low level of impurities.[4,8]

The focus of this article is on explaining how the metal alkylamide precursors are effective in ALD at low temperature.

Calculations using a periodic slab are carried out on a HfO_2 surface subjected to $Hf(NMe_2)_4$ and H_2O pulses. In this model, the Lewis acid-base reactions of precursor adsorption and by-product elimination are described. The effect of bridging O, bare O and OH as adsorption sites are considered. Under-coordinated oxygen are expected to have an important role during densification of precursor fragments. Densification is defined as the increase in density due to improved Hf−O packing, associated with an increase in coordination numbers of Hf and O from their molecular values (4 and 2 respectively) towards bulk solid values (7 and 4).[9] Moreover, H-transfer from sites adjacent to the adsorbed precursor is considered so as to see how those transfers change the reaction path in ALD.

It is clear that OH groups play an important role in growth reactions in oxide ALD, whether the co-reagent is H_2O or O_3 (protons are produced during oxidation of organic fragments in the latter case[10]). Different types of proton diffusion are inspected, to investigate whether multiple proton diffusion can facilitate dissociation of the fragment. We found that the way protons are diffusing between the surface and the adsorbed complex, as well as within the complex, reveals why low temperature ALD works in this case.

The intention of our work is to elucidate the mechanism of hafnium oxide ALD, by obtaining quantitative information on the energetics ΔE, ΔG and E_a of reactions between adsorbate structures during both the $Hf(NMe_2)_4$ pulse and the water pulse. We use density functional theory (DFT) to compute the reaction energetics of $Hf(NMe_2)_4$ adsorption, amide group dissociation and proton diffusion on a fully hydroxylated hafnium oxide surface. We also compute the reactions during the H_2O pulse, such as the interaction of H_2O with fragments of $Hf(NMe_2)_4$ precursor, explaining how the water molecule obtains higher coordination and becomes densified at the surface. The model thus describes chemical reactions throughout the ALD process, from the early stage of the $Hf(NMe_2)_4$ precursor with the substrate to obtaining bulk-like hafnium oxide at the end of the water pulse.

Computational details

To model the growth reactions of HfO_2 from HfX_4 (X = $N(CH_3)_2$) and H_2O, self consistent DFT was employed.[11] The reaction energies, activation energies and ab initio molecular dynamics (MD) of the system were calculated in a 3D periodic model utilizing VASP.[12] In these calculations, the electronic energies were approximated using the projected augmented wave (PAW)[13] description of atomic cores and the functional of Perdew, Burke and Ernzerhof (PBE).[14] The plane wave cutoff energy was 400 eV.[15] For Hf atoms $5d^2 6s^2$, N atoms $2s^2 2p^3$, O atoms $2s^2 2p^4$, and C atoms $2s^2 2p^2$ electrons were included as valence electrons. All calculations were closed shell since no unpaired electrons are expected in these calculations. The self-consistent steps were converged to an energy difference of 10^{-4} eV.

Geometries were optimized using the conjugate-gradient scheme[16] with no symmetry restraints and no fixed atoms to a convergence of gradients to less than 10^{-3} eV/Å. To compute ab initio thermodynamics, the translational entropy (S) of gas-phase molecules only were calculated[17] under the assumption that rotational, vibrational and surface contributions to S are approximately constant. TS^{transl} at T = 500 K were calculated to be 1.50, 1.21, and 0.49 eV for HfX_4, HX, and H_2O respectively. This allows Gibbs free energies ΔG of the reactions to be reported step by step.

Hafnium oxide has a different crystal structure at different temperatures.[18] The monoclinic phase is the most stable phase at low temperature, and our calculation showed that the (111) surface plane has the lowest energy. Therefore this direction has been regarded as a stable substrate for studying reactions during HfO_2 growth on HfO_2. The surface structure during actual ALD reactions is not known, but is certainly more complex. ALD produces amorphous or polycrystalline films of HfO_2, depending on precursor chemistry and growth temperature,[19] but the limitations of our periodic model do not permit us to simulate this. Converged values of surface energies of the (111) surfaces showed that four layers of HfO_2 is enough to be considered as the slab.[20] To avoid slab-slab interaction in the periodic model, 10 Å was regarded as the vacuum distance. The k-point sampling in reciprocal space was generated by the Monkhorst-Pack method:[21] $4\times4\times4$ and $4\times4\times1$ grid sizes were utilized for bulk and slab optimization respectively. For the hydroxylated

surface, we used a four-layered 2×2 supercell and so k-point sampling was reduced to $2\times2\times1$.

Ab initio MD calculations were carried out within the microcanonical ensemble.[22] The Verlet algorithm was used to integrate Newton's classical equations of motion for the ions. A time step of 1 femtosecond was found to be adequate for all frequencies of oscillation in the system. The calculations were done for 400 ionic steps. The initial temperature for assigning random velocities was varied from 300 to 600 K, in line with ALD experiments.

In our modeling, we are confronted with the obstacle of rare events.[23] For long periods of time (relative to our MD simulation) the system is trapped in one minimum and cannot escape from that minimum. To observe the transition to a new minimum, very long MD simulations would be needed, which would be inaccessible with current computational power. We therefore tried out other plausible configurations (candidate minimums) by hand and checked stability with optimization or ab initio MD. Occasionally, chemical reactions occurred rapidly from the chosen configurations and were observed during optimization or MD. In those cases, we then looked for pathways showing how the system reached those configurations.

To calculate activation energies between two minima, we used the nudged elastic band (NEB) approach[24,25] with climbing option. The conjugate gradient algorithm was found to be much faster than quasi-Newton methods to minimise forces in the NEB method and therefore conjugate gradient was employed for calculations. To compute the activation energy of HX desorption from surface-Hf with NEB, only the Hf$-$N bond length was stretched and all other degrees of freedom were optimised. Up to ten images were considered in those reaction paths. The maximum change in ionic coordinates between images was 0.30 Å. In proton diffusion, several reaction paths between each pair of minima were searched to find the minimum energy path. In the case of proton diffusion from oxygen to nitrogen, only the coordinates of the proton were fixed as it moved from one minimum to the other one. The maximum change in coordinates between images was 0.10 Å. For HX rotation, all atoms in the HX group were rotated around the Hf$-$N bond typically by 20° in every image.

Generally in ALD, we are looking for low reaction barriers, accessible at process temperatures

of around 500 K. In many cases, the barriers obtained were larger than 1 eV, and those are not reported here. For instance, for ligand rotation, the barrier is sensitive to whether the precursor is attached to O or OH. If attached to O, the precursor cannot move up from the surface and a higher barrier is obtained (1.78 eV) , which is too high to be relevant for ALD. Furthermore, if the rotational barrier in one direction is larger than in the other direction then we quote the lower value of E_a.

Results

End of H_2O pulse

Bare HfO_2 has many Lewis acid (Hf) and base (O) sites at the surface because of under-coordination. By contrast, at the end of the H_2O pulse in ALD, the surface is saturated with OH groups. In our model, we therefore added extra H_2O molecules to the bare (111) surface until we had obtained a hydroxylated surface. Those H_2O molecules are added to both top and bottom of the slab to minimise the slab dipole. The H_2O molecules initially are dissociated to H^+ and OH^-. Under-coordinated surface oxygen splits a proton from the water molecule and surface hafnium also gets a higher coordination number (c.n) due to bonding to the OH group. The bond length between the Hf (c.n = 7) and the terminal OH group at the surface (c.n = 2) is 2.06 Å which is lower than bond length between the Hf (c.n = 7) and O (c.n = 3), 2.17 Å. When hafnium and oxygen atoms achieve a sufficiently high c.n, they do not dissociate water molecules at the surface any more. In other words, when the surface is saturated by hydroxyl groups, there are no Lewis acid and base sites to dissociate water molecules. At this stage, water molecules can persist at the surface. The bond length between Hf of the surface and an adsorbed H_2O molecule is 2.42 Å. Those molecules are not tightly bonded to the surface and during ab initio MD simulation at 500 K they were seen to separate from surface. The NEB calculation shows 0.46 eV barrier for dissociation of H_2O from the 7 coordinated hafnium at the surface. The resulting model of the surface had a coverage of 5 OH/nm^2 and 2 H_2O/nm^2.

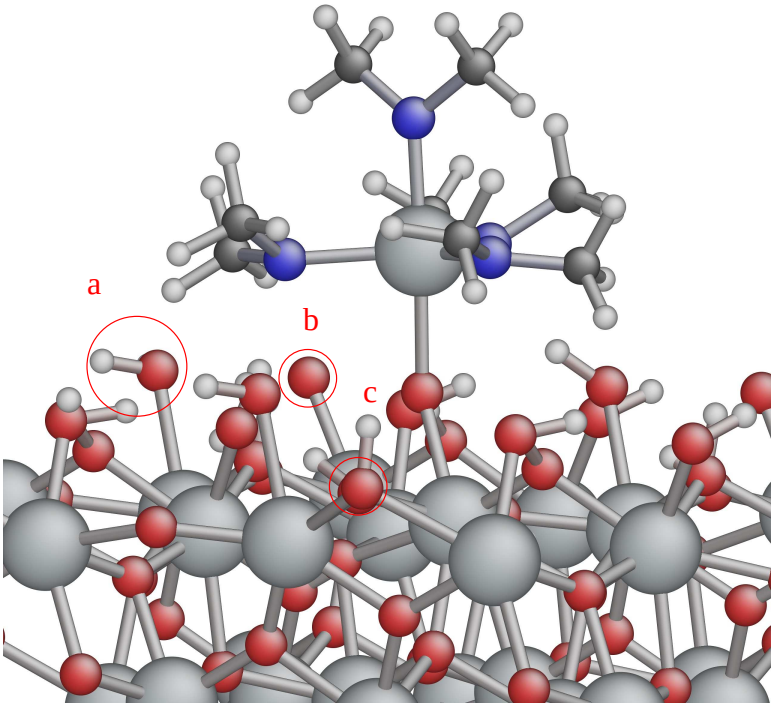


Figure 1: Optimized geometry for adsorption of HfX_4 molecule onto OH terminated HfO_2. Terminal hydroxyl group (a), terminal oxygen (b) and bridging oxygen (c) are highlighted. The HfX_4 is anchored to a terminal oxygen. (Red = O, Blue = N, White = H, large grey = Hf, small grey = C).

Adsorption during Hf pulse

Although unreactive towards H_2O, the OH-terminated surface has Lewis basic oxygen sites, i.e. those that can make a chemical bond by electron donation to the metal of the precursor. Those active sites can be sorted into terminal hydroxyl groups, terminal oxygen, and bridging oxygen (Figure 1). Terminal hydroxyl groups and terminal oxygen are one coordinated and bridging oxygen is two coordinated (excluding H). Our calculations show that the HfX_4 precursor cannot anchor to the bridging oxygen. Likewise, other oxygen atoms with even higher c.n are therefore inaccessible to the metal of the precursor. We find that the terminal oxygen and hydroxyl oxygen are able to make a dative chemical bond with Hf of the precursor.

ΔE were calculated for the mentioned sites (Table 1, reactions 3,4,5). If the change in entropy in the adsorption reaction is considered, which is essentially from translational entropy, then the chemisorption is energetically unfavorable. ΔG are respectively 1.37, 1.49, and 1.65 eV for reaction 3 to 5 (Table 1). The NEB calculation showed that the desorption barrier for ($HfX_4(s) \longrightarrow HfX_4(g)$) is 1.00 eV and during ab initio MD also no evidence of desorption was observed. Therefore the hafnium precursor is anchored to the surface in a metastable state at either site for periods of time that are long enough for further reactions to take place.

Proton diffusion (during either precursor pulse)

On the growing surface during ALD, protons may be bound to O or to N (of the ligand) and hence there are many proton diffusion paths, which can be sorted as diffusion from oxygen to oxygen, oxygen to nitrogen, and nitrogen to nitrogen. All proton diffusion types are shown in Table 1. In the calculations of proton diffusion, changes in entropy are small and can be ignored, so only changes in energy are reported. Different diffusion pathways have different activation energies.

We consider first proton diffusion from oxygen to oxygen in different situations (Table 1, reactions 1 and 2). Generally, we find that protons stay on under-coordinated oxygen. If we remove a proton from one-coordinated hydroxyl, the oxygen spontaneously dissociates a proton from a nearby H_2O molecule or from another hydroxyl with higher c.n (reaction 1). These proton trans-

Table 1: Diffusion barriers for protons in ALD and HfX_4 adsorption energies. E_a is activation energy and X = $N(CH_3)_2$. The 'dn' and 'up' indicate the position of proton on the nitrogen. surf-* means Hf precursor is anchored to * on the surface.

label	reaction	E_a (eV)	ΔE (eV)	explanation
1	$O_{c.n=1}(s) + OH_{c.n>1}(s) \rightleftharpoons OH_{c.n=1}(s) + O_{c.n>1}(s)$	0.00	0.00	—
2	$O_{c.n=m}(s) + OH_{c.n=m}(s) \rightleftharpoons OH_{c.n=m}(s) + O_{c.n=m}(s)$	0.75	0.00	m=1,2
3	$HfX_4(g) \rightleftharpoons HfX_4(s)$	1.00	-0.13	surf$-$O
4	$HfX_4(g) \rightleftharpoons HfX_4(s)$	1.00	-0.01	surf$-$OH
5	$HfX_4(g) \rightleftharpoons HfX_4(s)$	1.00	0.15	surf$-H_2O$
6	$HfX_4(s) + OH(s) \rightleftharpoons Hf(H_{dn}X)X_3(s) + O(s)$	0.05	-0.57	surf$-$OH
7	$Hf(H_{dn}X)X_3(s) + OH(s) \rightleftharpoons Hf(H_{dn}X)(H_{dn}X)X_2$	0.20	-0.19	surf$-$OH
8	$Hf(H_{dn}X)(H_{dn}X)X_2(s) + OH(s) \rightleftharpoons Hf(H_{dn}X)(H_{dn}X)(H_{dn}X)X(s) + O(s)$	0.30	-0.08	surf$-$OH
9	$Hf(H_{dn}X)(H_{dn}X)(H_{dn}X)X(s) \rightleftharpoons Hf(H_{up}X)(H_{dn}X)(H_{dn}X)X(s)$	0.51	-0.13	surf$-$OH
10	$Hf(H_{up}X)(X')X_2(s) \rightleftharpoons HfX(H_{up}X')X_2(s)^a$	0.59	-0.47	surf$-$OH
11	$Hf(H_{up}X)(H_{dn}X)X_2(s) \rightleftharpoons Hf(H_{up}X)(H_{up}X)X_2(s)$	0.49	-0.32	surf$-$OH
12	$Hf(H_{up}X)(H_{up}X)(H_{dn}X)X(s) \rightleftharpoons Hf(H_{up}X)(H_{up}X)(H_{up}X)X(s)^b$	0.42	-2.30	surf$-$OH
13	$Hf(H_{dn}X)(H_{dn}X)X(s) \rightleftharpoons Hf(H_{up}X)(H_{dn}X)X(s)$	0.38	0.00	surf$-$OH
14	$HfX_2(s) + OH(s) \rightleftharpoons Hf(H_{up}X)X(s) + O(s)$	0.91	-0.34	—
15	$Hf(H_{up}X)X(s) + OH(s) \rightleftharpoons Hf(H_{up}X)(H_{up}X)(s) + O(s)$	0.88	-0.27	—

[a] X′ shows the topmost nitrogen.

[b] densified precursor, this precursor is not stable at the surface.

fers are barrierless and take place during optimization. So we conclude that protons move quickly to the oxygen with lowest c.n. However, there is a 0.75 eV barrier for proton diffusion from one or two coordinated oxygen to a similar oxygen with the same c.n (reaction 2).

We investigated whether protons diffuse from the surface to sub-surface layers. A proton could not be optimized on the four coordinated oxygen of the sub-surface and it transferred spontaneously to the three coordinated oxygen. In another case, the existence of a proton on a four coordinated oxygen caused the bond between hafnium and that oxygen to break, with an overall cost for proton transfer of ΔE = +1.03 eV. Therefore during the processes of ALD, protons stay on top of the HfO_2 surface and do not diffuse into sub-surface layers of highly coordinated O.

Another type of proton diffusion is from oxygen to the ligand. For a bulky ligand like amide, there are various geometries for the protonated ligand HX. The NEB calculations showed that the rate of proton diffusion strongly depends on the distance that proton hops from O to N. For example, we obtained a 1.35 eV barrier for diffusion of the proton across the distance 2.43 Å, while we obtained various values from 0.05 to 0.39 eV for the much shorter diffusion distance $\sim$ 0.7$\pm$0.05 Å (Table 1, reactions 6, 7, and 8) (The corresponding O$-$N distances are similar, i.e. 2.8-3.0 Å). During ab initio MD or NEB calculations, these protons move up or down between the surface and the ligand. The bond length between Hf of the precursor and surface OH (c.n = 3) is changed from 2.26 to 2.18 and 2.07 Å due to the first and second proton diffusion from the surface diffusion to the nitrogen (Table 1, reaction 6, 7).

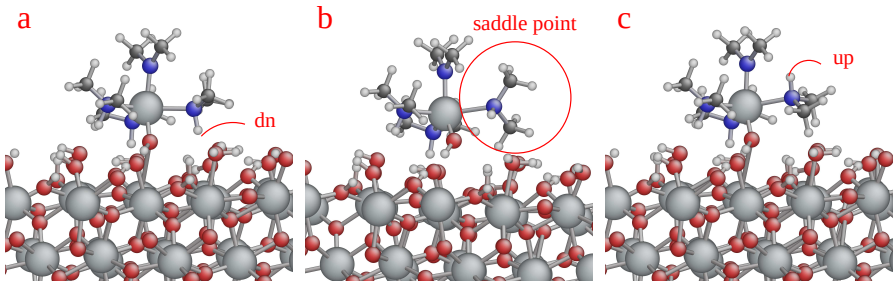


Figure 2: Rotation of protonated ligand from $Hf(H_{dn}X)(H_{dn}X)(H_{dn}X)X$ to $Hf(H_{dn}X)(H_{dn}X)(H_{up}X)X$, X = $N(CH_3)_2$ where the 'dn'(a) and 'up'(c) show the orientation of the proton on nitrogen relative to the surface. The saddle point is indicated in (b).

Protons can also diffuse through the adsorbate via rotation of the protonated ligand HX (Figure 2). The proton on nitrogen can be oriented down towards the surface or up away from the surface. Those locations are indicated by 'dn' and 'up' respectively in Figure 2. Several reaction paths were regarded to find how the proton moves. The ligand needs space to rotate and this is facilitated by lengthening of the Hf$\cdots$O bond between the entire precursor and the surface. Such lengthening apparently costs more energy for surf$-$O$-$Hf ($E_a \sim 1.78$ eV for rotation of HX) than for surf$-$OH$-$Hf ($E_a \sim 0.51$ eV) (Figure 2 and Table 1, reaction 9). In other words, a higher barrier exists towards amide rotation when the precursor is attached to terminal oxygen, and this is probably because terminal oxygen does not allow the precursor to move away from the surface as easily as OH does. The adsorption mode thus affects the rate of proton diffusion and hence of ligand elimination and ALD growth. The bond length between the Hf of the precursor and the surface OH (c.n = 3) is slightly decreased from 2.18 to 2.15 Å because of the rotation of the protonated ligand in $Hf(H_{dn}X)X_3 \rightleftharpoons Hf(H_{up}X)X_3$.

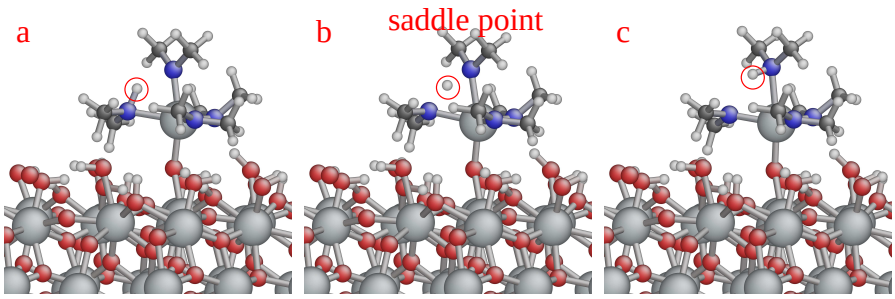


Figure 3: The highlighted proton diffuses from nitrogen to the topmost nitrogen. The saddle point is indicated in the middle snapshot (b).

Proton diffusion from nitrogen to nitrogen within the adsorbate after proton rotation is the other diffusion type (Figure 3). E_a = 0.59 eV was calculated by NEB for this diffusion (Table 1, reaction 10).

Table 2: Activation energy for HX desorption from protonated HfX_4 and HfX_3 configurations i.e. probably Hf pulse. ΔG is free energy at T = 500 K and E_a is activation energy. X = $N(CH_3)_2$ and the 'dn' and 'up' show the position of proton on the nitrogen.

label	reaction	E_a (eV)	ΔE (eV)	ΔG^{500K} (eV)
1	$Hf(H_{dn}X)X_3(s) \rightleftharpoons HfX_3(s) + HX(g)$	0.89	-0.35	-1.56
2	$Hf(H_{up}X)(H_{dn}X)(H_{dn}X)X(s) \rightleftharpoons Hf(H_{dn}X)(H_{dn}X)X(s) + HX(g)$	0.89	-0.94	-2.15
3	$Hf(H_{up}X)(H_{up}X)(H_{dn}X)X(s) \rightleftharpoons Hf(H_{up}X)(H_{dn}X)X(s) + HX(g)$	0.39	-0.44	-1.65
4	$Hf(H_{up}X)(H_{up}X)(H_{up}X)X(s) \rightleftharpoons Hf(H_{up}X)X(s) + 2\,HX(g)$	0.00	-1.91	-4.33
5	$Hf(H_{dn}X)X_2(s) \rightleftharpoons HfX_2(s) + HX(g)$	1.69	-1.18	-2.39
6	$Hf(H_{up}X)(H_{up}X)(H_{dn}X)(s) \rightleftharpoons Hf(H_{up}X)(H_{dn}X)(s) + H_{up}X(g)$	1.09	-2.92	-4.13
7	$Hf(H_{up}X)(H_{up}X)(H_{dn}X)(s) \rightleftharpoons Hf(H_{up}X)(H_{dn}X)(s) + H_{up}X(g)$	1.07	-2.92	-4.13
8	$Hf(H_{up}X)(H_{up}X)(H_{dn}X)(s) \rightleftharpoons Hf(H_{up}X)(H_{up}X)(s) + H_{dn}X(g)$	1.73	-2.92	-4.13

Elimination of ligands and densification

The common assumption about the ALD mechanism is that proton transfer to a ligand, X(s) $\longrightarrow$ HX(s), is followed rapidly by desorption of the protonated ligand, HX(s) $\longrightarrow$ HX(g), before the next proton transfer step to the remaining precursor fragment.[17] Accordingly, the activation energy for desorption of the first HX from $Hf(H_{dn}X)X_3$ was calculated by NEB to be E_a = 0.89 eV (Table 2, reaction 1).

Here, we test the alternative mechanism, where multiple proton transfer gives $Hf(HX)(HX)X_2(s)$ or Hf(HX)(HX)(HX)X(s) etc., followed later by desorption of HX(g) (Table 1, reactions 11, 12, and 13). As shown in Figure 4, the Hf−N distance increases from 2.2 to 2.6 Å as a result of protonation of the amide, showing that there is still substantial bonding between the neutral protonated amine (dn) and the Hf centre. Reaction 2 in Table 2 is dissociation of $H_{up}X$ from $Hf(H_{up}X)(H_{dn}X)(H_{dn}X)X$. The activation energy E_a = 0.89 eV for this reaction is the same as that computed for reaction 1 in Table 2. To achieve this, a proton initially diffuses from the surface to nitrogen, then rotates to the 'up' position, and diffuses to the highest nitrogen, before finally desorbing as HX. Those diffusion steps are explained above.

These data show that rotation of the protonated ligand (Table 1, reactions 9, 11, and 12) has a

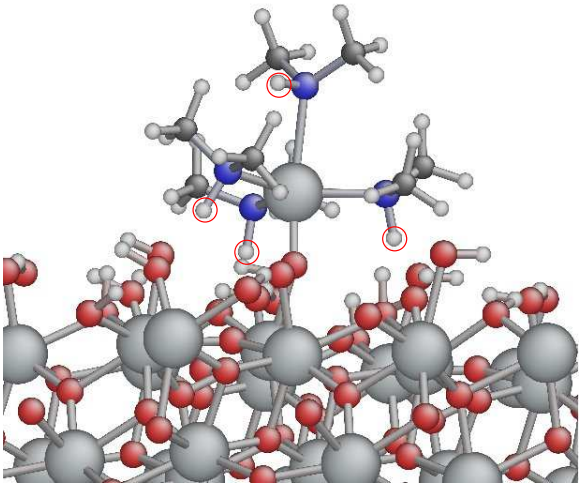


Figure 4: The Hf(H_{up}X)(H_{dn}X)(H_{dn}X)(H_{dn}X) precursor at the surface. Because of multiple proton diffusion, the topmost bond between Hf−N is stretched. Red circles show the diffused protons from the surface to the nitrogen.

much higher rate than dissociation of H_{up}X from the precursor (Table 2, reactions 1 and 2). For instance, using the computed E_a in the Arrhenius equation for 500 K shows that the rate of Table 1 reaction 9 is 4 orders of magnitude higher than Table 2 reaction 2.

In terms of activation energy the most likely desorption is reaction 3 in Table 2, in which three protons have diffused to the precursor and two amides have rotated upwards. These protons are highlighted in Figure 5. The activation energy was calculated by NEB to be 0.39 eV. The rate of this reaction is therefore 6 orders of magnitude higher at 500 K than dissociation of H_{dn}X in Table 2 reaction 1 and 2. In other words, when the precursor has the Hf(H_{up}X)(H_{dn}X)(H_{dn}X)X configuration, the next proton rotation dn $\longrightarrow$ up makes the desorption of H_{up}X easier. We have observed that HX dissociates from Hf(H_{up}X)(H_{up}X)(H_{dn}X)X during ab initio MD (Figure 5) at T = 500 K for 0.4 ps. Therefore H_{up}X is not tightly bonded to the metal when another H_{up}X is present. The bond length between Hf of the precursor and the surface O (c.n = 2) changes from 1.80 Å in Hf(H_{up}X)(H_{dn}X)(H_{dn}X)X to 1.82 Å in Hf(H_{up}X)(H_{up}X)(H_{dn}X)X.

When the precursor chemisorbs to the surface, hafnium makes a bond with oxygen at the

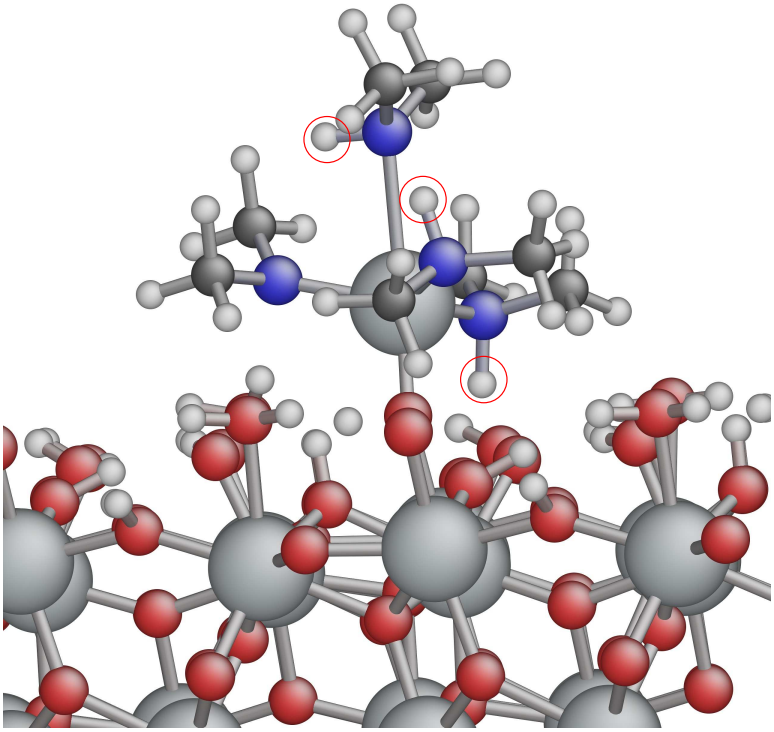


Figure 5: The Hf(H_{up}X)(H_{up}X)(H_{dn}X)X precursor at hafnium oxide surface. The topmost HX is dissociating from hafnium during ab initio MD calculation. Red circles show the diffused protons from surface to the ligands.

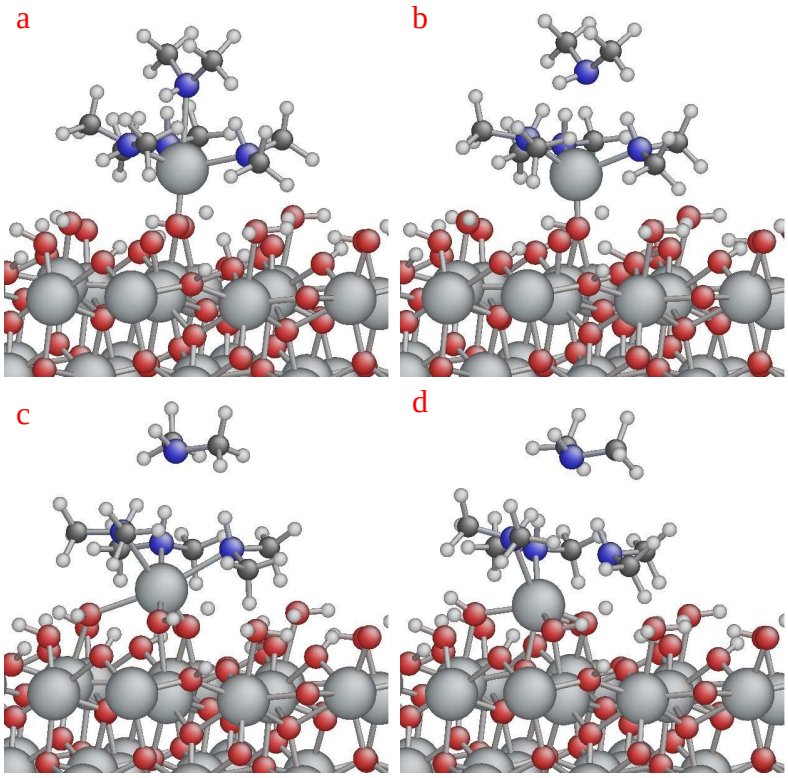


Figure 6: Snapshots from optimization of Hf(H_{up}X)(H_{up}X)(H_{up}X)(H_{up}X) configuration. Hf moves down into the surface and becomes strongly attached to a total of four O atoms in the surface as 2 HX desorb.

surface and hafnium becomes 5 coordinated. The bonds between N and Hf may have some covalent character. After the first elimination, the hafnium is 4 coordinated. With further elimination of HX, hafnium bonds with more oxygen at the surface, becomes more highly coordinated and thus densifies towards the bulk c.n.

Rotation of the third proton from $Hf(H_{up}X)(H_{up}X)(H_{dn}X)X$ to $Hf(H_{up}X)(H_{up}X)(H_{up}X)X$ (Table 1, reaction 12) causes spontaneous desorption of two HX at the same time (Table 2, reaction 4). In a similar way, as shown in Figure 6, Hf moves spontaneously downwards into the surface during optimization of $Hf(H_{up}X)(H_{up}X)(H_{up}X)(H_{up}X)$ and the $Hf(H_{up}X)(H_{up}X)$ fragment densifies to the surface (i.e. c.n. of Hf increases from 4 to 6). The HX desorption step is barrierless in these cases.

As indicated in Table 2, multiple proton diffusion to N and rotation to $H_{up}X$ reduces the activation energy for HX desorption. Upwardly-oriented HX dissociates readily from $Hf(H_{up}X)(H_{up}X)(H_{dn}X)$ during ab initio MD. Therefore as already observed above for HfX_4 configurations, the diffusion of multiple protons to the adsorbate increases the HX dissociation rate, in the case of ligands like X = amide. The bond length between the Hf of the precursor and the surface O (c.n = 2) changes from 1.91 Å for HfX_3 to 1.87 and 1.81 Å in $Hf(H_{dn}X)X_2$ and $Hf(H_{dn}X)(H_{dn}X)X$ respectively. This bond length is not changed in $Hf(H_{up}X)(H_{up}X)(H_{dn}X)$.

A substantial energy difference ΔG= -4.1 eV at T = 500 K is seen for dissociation of the second HX (Table 2 reactions 6). This energy difference is higher than the first dissociation and this probably comes from densification, as shown in serial snapshots in Figure 7. Loss of the second HX allows hafnium to move down into the surface and bond with under-coordinated oxygen. As the remaining amide groups are bulky in HfX_2 configurations, we found a small barrier towards this densification step, which is overcome during ab initio MD. After densification, the amide groups in HfX_2 are bent up (Figure 7d) and so the next proton can be expected to travel a larger distance than in HfX_3 to bind to N and detach HX from hafnium. Indeed, calculations show a larger barrier than before for proton diffusion from oxygen to nitrogen (Table 1, reaction 14, 15).

When the precursor is densified to the surface, the Hf c.n increases from 3 to 5. This changes the rate of subsequent dissociation of HX because we find a strong dependence of activation en-

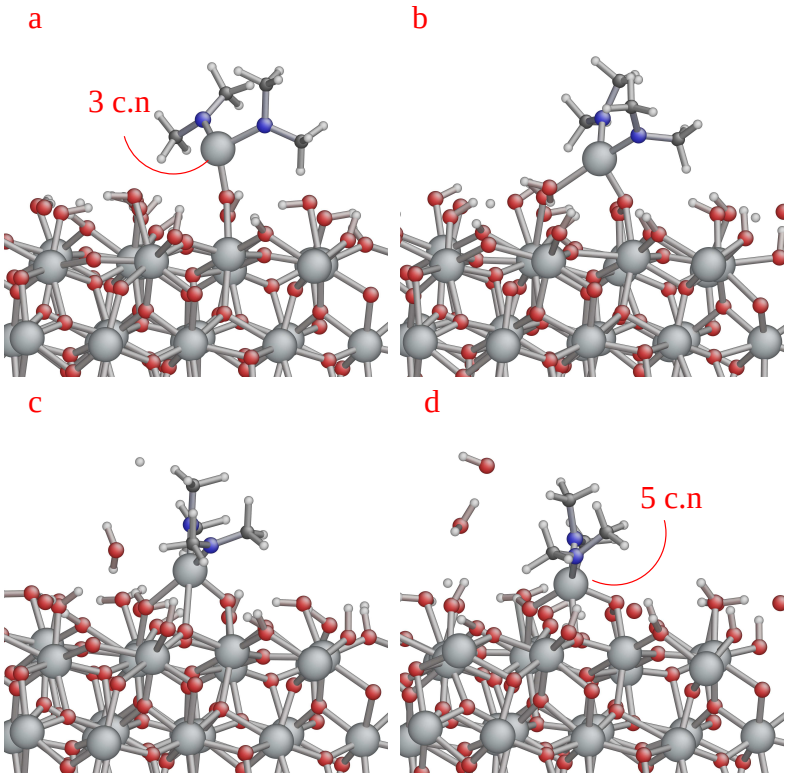


Figure 7: By densification, the c.n of Hf in the precursor is increased as HfX_2 becomes strongly attached to 3 oxygen atoms at the surface. Snapshots are from ab initio MD at T = 500 K for 0.4 ps.

ergies on c.n of Hf for the crucial reaction steps of HX rotation and desorption. The activation energy E_a = 1.13 eV was calculated for HX dissociation from Hf(H_{dn}X)X (Table 3, reaction 1). After densification, hafnium has a higher c.n, which may explain why this dissociation has a lower barrier than Hf(H_{dn}X)X_2 (Table 2, reaction 5). In the case of Hf(H_{up}X)X, E_a = 0.89 eV is calculated for HX desorption (Table 3, reaction 2). Multiple diffusion increases the dissociation rate in these configurations also (Figure 8): Hf(H_{dn}X)(H_{up}X), has a lower barrier E_a = 0.30 eV, (Table 3, reaction 3) than Hf(H_{dn}X)X.

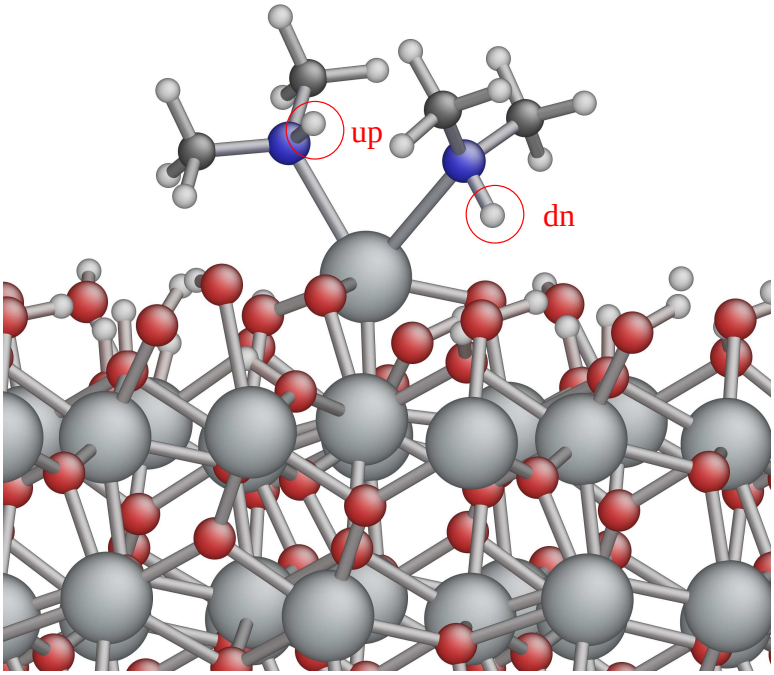


Figure 8: Optimized Hf(H_{dn}X)(H_{up}X) attached to 3 oxygen atoms at the surface where the 'dn' and 'up' show the orientation of the proton on nitrogen relative to the surface.

As indicated in Table 3 reaction 3, exothermic ΔG = -0.40 eV was obtained for HX desorption from HfX_2. However, for dissociation of the last HX, the reaction is endothermic, ΔG = 0.53 eV, with a substantial activation barrier E_a=1.64 eV (Table 3, reaction 8). Hence the energetics favour Hf(HX) as the most likely fragment at the end of the HfX_4 pulse, if there are sufficient surface protons.

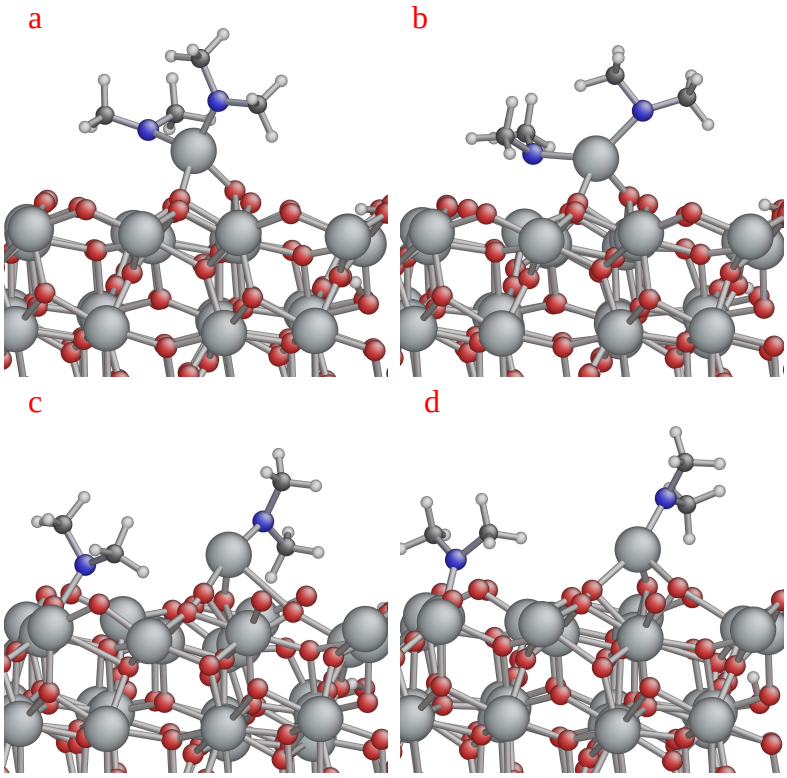


Figure 9: The amide group of the densified HfX_2 was transferred to under-coordinated hafnium at the surface; snapshots are from ab initio MD calculation, starting at T = 500 K and running for 0.4 ps.

Table 3: Reaction routes for HX dissociation after densification, and ligand exchange with oxygen, ΔG is free energy at T = 500 K and E_a is activation energy.

label	reaction	E_a (eV)	ΔE (eV)	ΔG^{500K} (eV)
1	$Hf(H_{dn}X)X(s) \rightleftharpoons HfX(s) + HX(g)$	1.13	1.36	+0.15
2	$Hf(H_{up}X)X(s) \rightleftharpoons HfX(s) + HX(g)$	0.89	1.03	-0.17
3	$Hf(H_{dn}X)(H_{up}X)(s) \rightleftharpoons Hf(H_{up}X)(s) + HX(g)$	0.30	0.80	-0.40
4	$4\,HfX(s) + H_2O(g) \rightleftharpoons 3\,HfX(HfH_{up}X)(s)^a + OH(s)$	0.00	-2.24	-1.75
5	$3\,HfX(HfH_{up}X)(s) + H_2O(g) + O(s) \rightleftharpoons 3\,HfX(HfH_{up}X)(s) + OH(s) + OH(s)$	—	-1.56	-1.07
6	$3\,HfX(HfH_{up}X)(s) + H_2O(g) \rightleftharpoons 2\,HfX(HfH_{up}X)(HfH_{up}X)(s) + OH(s)$	—	-1.19	-0.70
7	$2\,HfX(HfH_{up}X)(HfH_{up}X)(s) + H_2O(g) \rightleftharpoons HfX(HfH_{up}X)(HfH_{up}X)(HfH_{up}X)(s) + OH(s)$	—	-1.25	-0.76
8	$Hf(HX)(s)(c\cdot n = 5) \rightleftharpoons Hf(s)(c\cdot n = 4) + HX(g)$	1.64	1.74	+0.53
9	$Hf(HX)(s)(c\cdot n = 6) \rightleftharpoons Hf(s)(c\cdot n = 5) + HX(g)$	0.83	0.80	-0.40
10	$Hf(HX)(s)(c\cdot n = 7) \rightleftharpoons Hf(s)(c\cdot n = 6) + HX(g)$	0.56	-0.14	-1.35

[a] in the case of HfX there is no difference between 'dn' and 'up' proton

Another interesting reaction is transferring X from the adsorbed fragment HfX_2 to another under-coordinated Hf at the surface. As shown in Figure 9, HfX_2 releases a ligand, which is transferred to the neighbouring hafnium and changes it from c.n = 4 to c.n = 5. This mechanism is observed during ab initio MD, indicating a small barrier.

Start of H_2O pulse

As was mentioned above, the most probable configuration for the metal precursor is predicted to be HfX or Hf(HX) at the end of the metal pulse. Therefore, during the subsequent water pulse, adsorbing H_2O interacts mostly with HfX (c.n = 4 or 5 for Hf). In our models, we attached H_2O to HfX via $O\cdots Hf$ bonding (Figure 10a), but when we have low population of exposed Hf at the surface, the attached H_2O is not dissociated and desorbs spontaneously from the system (Figure 10b). It seems that there are not enough active sites on the surface to dissociate H_2O into OH^- and H^+. In the case of HfX_2, the problem is worse because of steric hindrance by X with

H_2O. Moreover, other Hf in the sub-surface layers are 6 or 7 coordinated and so cannot effect dissociation of OH from H_2O.

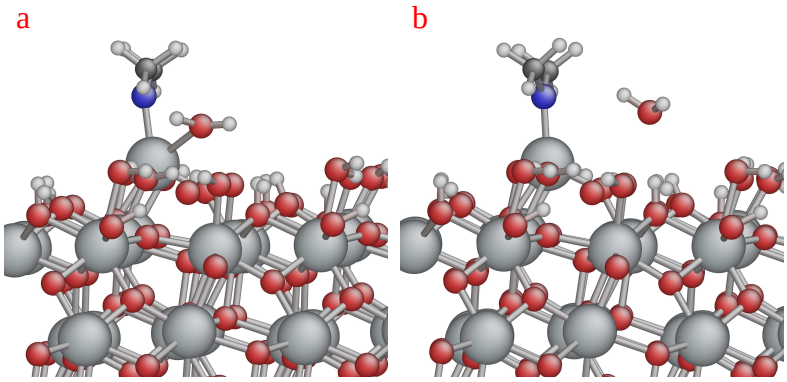


Figure 10: The H_2O molecule is not dissociated when there are not enough Lewis acid and base sites in terms of number; snapshots are from optimization.

However, a cluster of HfX leads to dissociation of adsorbed H_2O molecules. For instance, four HfX is considered as such a cluster. In Figure 11a, four HfX are optimized on adjacent sites (Hf$\cdots$Hf = 3.3-5.2 Å). We proceeded by adding H_2O molecules one by one to Hf atoms within the 4 HfX cluster at the surface (Figure 11b). As indicated in Table 3, reaction 4, the first H_2O molecule is spontaneously dissociated to H^+ and OH^- during optimization. The proton is bound to N (Lewis base) as HX and the hydroxyl group is attached to Hf (Lewis acid). For the second H_2O, dissociation of the H_2O molecule does not take place instantly. So the H_2O molecule was taken apart to OH^- and H^+ by hand, and the new geometry was optimized (Table 3 reaction 5). This time the proton forms a bond to under-coordinated O at the surface. Indeed, occasionally both protons of the H_2O molecule were transferred to surface O and left two coordinate oxygen bridging between under-coordinated hafnium. For the next two adsorbing H_2O molecules (Table 3 reactions 6 and 7), the proton was optimized on nitrogen and the remaining hydroxyl group was bridging between under-coordinated hafnium. As there are many active sites (basic and acidic sites) in this surface model, calculation of activation energies for these steps was difficult to manage.

As tabulated in Table 3 from reactions 4 to 7, ΔE and ΔG are both negative for the dissociative chemisorption of H_2O. From reactions 4 to 6, whenever we add more H_2O molecules to the

surface, ΔG and ΔE become less negative. This reduction seems to accompany the loss of Lewis acid and base sites through increased coordination to H_2O.

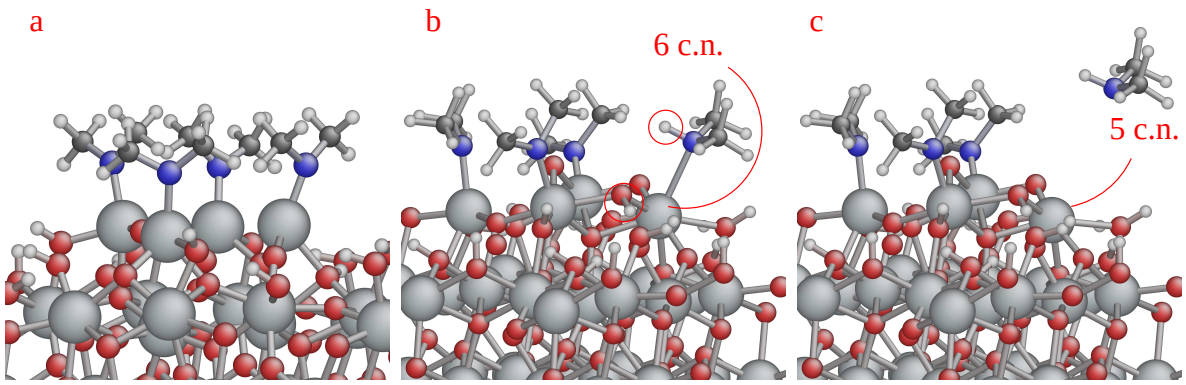


Figure 11: (a) The cluster of four HfX (b) The upper-most oxygen originally adsorbed as H_2O where red circles show typical OH and H from H_2O dissociation (c) Dissociation of HX from six coordinated Hf during the water pulse.

For HX loss, the opposite effect is seen in reactions 8 to 10 (Table 3) where ΔG becomes more negative as Hf c.n increases. In other words, repeated adsorption of H_2O molecules increases the c.n of Hf and is accompanied by the simultaneous dissociation of more and more HX from the surface. The activation energy is reduced from 1.64 eV to 0.56 eV for the last HX dissociation from Hf(HX) (Table 3 reactions 8 and 10). In the case of Figure 11b, $3H_2O$ were added and optimized. The E_a for loss of HX is 0.83 eV when Hf is six coordinated. Another H_2O molecule was added to the c.n = 6 hafnium that is shown in Figure 11b producing Hf with c.n = 7 with oxygen (Figure 12a). E_a = 0.56 eV is the activation energy for the last HX dissociation (Table 3, reaction 10).

Discussion

Ab initio calculations show that the Hf of the precursor adsorbs by making a dative bond with the Lewis acid sites at the surface. Formation of Hf−O bonds is energetically favorable. The existence of low coordinated O or OH is necessary for the dative bond to persist. The dative bond between the

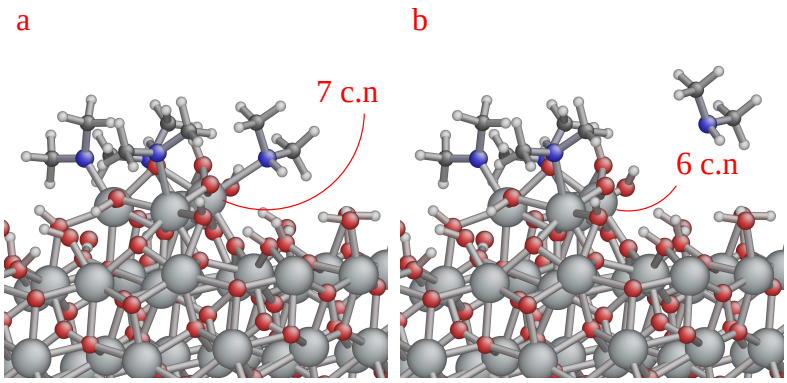


Figure 12: Dissociation of HX from seven coordinated hafnium during water pulse. Four oxygen (originally adsorbed as H_2O) are coordinated to the cluster and dissociation of HX from the resulting 7-coordinate Hf is more favourable than the situation in Figure 11.

Hf of the precursor and high coordinated O (c.n = 2) is not strong enough to preserve it for further reactions. The low and high coordinated O sites are created by decomposition of H_2O molecules during the H_2O pulse. Their equilibrium population essentially depends on the temperature of the substrate, which rules the rate of adsorption and finally the rate of growth in ALD. We could not find any reaction path for other adsorption modes of HfX_4 or for direct reactions between X of gas-phase HfX_4 and surface protons. The existence of the Hf−O dative bond is the necessary prerequisite for HX elimination.[26]

As the existence and mobility of Brønsted acidic protons is crucial in the ALD of oxides, various proton diffusion pathways are inspected (Table 1). Proton diffusion from oxygen to oxygen has various barriers, which change according to the c.n of oxygen. Generally protons remain on low coordinated oxygen, and therefore remain primarily at the surface rather than in the bulk. The existence of protons at the surface makes them available as co-reagents for the dissociation of ligand fragments.

The proton diffusion from oxygen to ligand nitrogen is the other type of proton diffusion. In our simulations, this proton hops frequently between oxygen and nitrogen and may be thought of as a shared proton between the oxygen and nitrogen. The desorption barriers of the fragment $H_{dn}X$ are relatively large, but are lowered by a factor of 2-3 by rotation of the protonated ligand to $H_{up}X$

(Table 1, reactions 9, 11, and 12 respectively), hence facilitating the desorption of the fragment $H_{up}X$. For all proton diffusion pathways, which are tabulated from reaction 6 to 13 in Table 1, the barriers are lower than the desorption barrier for $H_{dn}X$ (Table 2 reaction 1 and 2), which makes proton diffusion more probable than desorption of $H_{dn}X$ at the initial stage of precursor adsorption. In other words, multiple ligands become protonated before desorption commences.

Proton diffusion from the O of surface to the N of HfX_4 shows relatively low barriers and exothermic reactions energies (Table 1, reactions 6, 7, and 8). However, these proton diffusion barriers in HfX_2 are much higher than in HfX_4, at least for smooth surfaces (Table 1, reactions 14 and 15), because the proton must then travel a larger distance from O to attach to the N. However, if HfX_2 is densified into the sub-surface layers, then Hf is surrounded by more oxygen than at the smooth surface. In this case, the proton may travel a shorter distance to attach to the nitrogen than on the smooth surface. The proton diffusion barrier therefore is lower. An alternative route to protonated HfX_2 is by repeated loss of HX from larger protonated fragments such as $Hf(H_{up}X)(H_{up}X)(H_{up}X)(H_{dn}X)$. The resulting $Hf(H_{up}X)(H_{dn}X)$ species can densify directly, without the need for proton diffusion.

However, if Hf of the precursor is not coordinated to enough oxygen from the surface, for instance if it bonds to just two oxygen atoms, in spite of multiple diffusion, the HfX_2 or $Hf(HX)_2$ configuration keeps both ligands. This illustrates the link between ligand loss and coordination to the surface, as already computed by Zydor and Elliott for Ti precursors.[26]

Diffusion of protons from the surface oxygen to the nitrogen in ligands weakens the bonds between hafnium and ligands. Then, as noted above, rotation of protonated ligand dn $\longrightarrow$ up lowers the activation energy for HX desorption significantly. The more protonated ligands that rotate, the more rapidly the dissociation of HX proceeds. In the extreme case, we observed that two ligands spontaneously dissociated from $Hf(H_{up}X)(H_{up}X)(H_{up}X)X$ and Hf simultaneously densified to the surface. In other words, the system prefers to pass several low barriers instead of few high barriers in ALD. When the temperature is increased, those pathways with high barriers become more active. For instance, thermally-activated decomposition reactions that do not need co-reagents such as H^+

(i.e. standard chemical vapour deposition) may become active at higher temperatures. However, we have not computed such reactions here.

Hf in HfX_4 is bound to a single O and so is 5 coordinated. By loss of a ligand, it becomes 4 coordinated HfX_3. We find that dissociation of another HX from HfX_3 configurations is harder than from HfX_4 ones. (Table 2, reactions 1 and 5), showing that second elimination is harder in ALD. The other interesting point is the effect of ligand rotation on the desorption of HX from $Hf(H_{up}X)(H_{up}X)(H_{dn}X)$. As indicated in Table 2, reactions 6 and 7 have similar activation energy for $H_{up}X$ dissociation, while the activation energy for $H_{dn}X$ dissociation in reaction 8 is too high for this reaction to be active in ALD. Hence, the proton rotations in HfX_3 configurations also change the dissociation rate.

The bonding between the Hf of the precursor and the low coordinated O changes in response to proton diffusion from the surface to the ligands and rotation of protonated ligand. For instance, multiple proton diffusion decreases the Hf−O bond length from 2.26 Å in HfX_4 to 1.82 Å in $Hf(H_{up}X)(H_{up}X)(H_{dn}X)X$, which is lower than the normal distance between Hf and O in the bulk structure (2.17 Å). This effect appears to be primarily due to the proton diffusion from the surface to the complex, while the rotation of the protonated ligand is only slightly influential.

We observe that densification is the primary energetic driving force at the surface. Substantial energy gain can be seen to accompany the formation of new Hf−O bonds in reactions 4 to 8 in Table 2. Densification is reported here for a smooth surface, where Hf of the precursor bonds to 3 or 4 oxygen atoms at the surface. Densification may also happen in sub-surface layers during ALD growth, where Hf and O rearrange so as to obtain more mutual bonding partners, increasing their coordination and density closer to bulk values. In this case, we expect that densification is even more energetically favorable. This leads us to speculate that there will also be a strong driving force for Hf and O ions, once freed of ligands or protons, to migrate from the surface to sub-surface vacancies, thus densifying and completing those layers into bulk-like HfO_2. This would explain the excellent conformality that is achieved in ALD, despite the sub-monolayer rate of growth per cycle. Each ALD cycle thus consists of two simultaneous modes of deposition: completion of

high-density sub-surface layers and decoration of the surface with a low-density film. Of course, the situation may be different during the first few cycles of 'incubation' on a substrate.

Based on the computed energetics, HfX is the most probable configuration in the Hf pulse and desorption of this final HX is an endothermic reaction (Table 3 reaction 8). This seems to be because HfX is relatively under-coordinated. One bond from X and 3 or 4 bonds from oxygen (on a smooth surface) make Hf 4 or 5 coordinated. Desorption of the last ligand only becomes possible if Hf can coordinate to more oxygen, either during the oxygen pulse or by densification into a position with a higher number of surrounding oxygen (Table 3, reactions 8, 9, and 10). Because ideal ALD is symmetric with respect to pulses, the energetics also allow us to identify the most probable surface species saturating the surface at the end of the H_2O pulse. This is low-coordinated hydroxyl, with just one bond to the surface, which resists any type of proton transfer reaction (Table 1, reaction 1). Only during the next precursor pulse does adsorption of HfX_4 allow the coordination number of such OH groups to increase, facilitating proton transfer and densification.

Our calculations show that the H_2O molecule in the oxygen pulse can only adsorb by attaching to a pair or cluster of neighbouring HfX, which is followed by decomposition of the H_2O molecule (Table 3 reaction 5). Adsorption of H_2O to a single HfX is not energetically favoured (Figure 10), indicating that the presence of X makes HfX a weak Lewis acid. Also, no evidence of a direct reaction between a proton of the gas phase H_2O molecule and surface ligands was observed, again confirming that chemisorption is needed before HX elimination. If such clusters of HfX do not form in the Hf pulse, which may happen in low temperature or on different interfaces, then H_2O cannot adsorb efficiently in the oxygen pulse. In general, a low number of Lewis acid and base sites after the Hf pulse leads to a low rate of H_2O deposition in the O pulse.

Repeated decomposition of H_2O leads to an increase in c.n of Hf and O in the cluster. Simultaneously, the densification of Hf and O in the cluster causes a reduction in the barriers to HX desorption (Table 3), and the rate of desorption of HX is increased. For this reason, previously inert Hf(HX) can be eliminated in the H_2O pulse. Depletion of HX from the cluster in turn allows

further densification: Hf gains c.n up to 7 by densification with surrounding O while the oxygen obtains wide range of c.n from 1 to 4.

At this stage, the possibility of association of $H^+ + OH^-$ into H_2O molecules is raised. According to our calculations, terminal -OH_2 with the low coordination of oxygen are more likely to desorb than bridging -OH_2- especially as the temperature is raised. As noted previously, terminal O is the most reactive towards HfX_4 adsorption in the next Hf precursor pulse and so the rate of ALD growth per cycle would be lowered as a result of the reduction in adsorption sites. In addition, H_2O desorption depletes the surface of reactive protons for ALD.

In our slab model, under-coordinated surface atoms (oxygen in the hafnium pulse and hafnium in the oxygen pulse) change the activation energies and free energies for reactions in their vicinity, reactions such as desorption of ligands and ligand exchange. Although they appear to be spectators in these reactions, in fact these under-coordinated atoms strongly affect the reaction pathways and energetics, often changing them from endothermic to exothermic reactions. For instance, the substantial gain in energy during the densification process is from under-coordinated atoms. These under-coordinated atoms are ignored in calculations using more limited models.[5,6]

Conclusion

In this paper, we used DFT slab models to investigate the ALD reactions for growth of HfO_2 from $Hf(NMe_2)_4$ and H_2O. We include all steps, from the early stage of adsorption of each ALD precursor to the densification of multiple atoms into bulk-like HfO_2 layers. The resulting reactions, which explain the fundamental chemistry of ALD at low temperatures (below 500 K), are outlined below.

Adsorption: Chemisorption of precursors is only possible at surface sites of sufficient Lewis activity, namely terminal O and OH for $Hf(NMe_2)_4$ and $(Hf(NMe_2))_x$ ($x \geq 2$) cluster (e.g. dimers) for H_2O. Saturated surfaces do not have these sites and so resist further adsorption. This explains the self-limiting reactions that distinguish ALD from other techniques.

Multiple proton diffusion: We propose the diffusion of multiple protons to the amide ligands of the Hf precursor before desorption of protonated ligands takes place. The activation energy calculations show that repeated proton diffusion from the surface to the amide ligand and rotation of the protonated amine is more energetically accessible than the simple elimination of the amine in the initial stage. Due to multiple proton diffusion to the fragments, the dative bonds between Hf and N are weakened. This reduction in bond strength facilitates the desorption of fragments from the precursor. The resulting activation energies for protonation and desorption of ligands are low enough that these reactions can take place in low temperature ALD. Multiple proton diffusion is seen in all the stages of ligand elimination.

Densification: Loss of a proton from oxygen frees it up for bonding to Hf of the precursor. Protonation of ligands, and especially desorption of ligands, frees up Hf for bonding to surface oxygen. Decomposition of H_2O at the surface also increases the coordination of Hf and O. These effects are termed 'densification', as they bring Hf−O packing closer to the bulk scenario. Densification is hence accompanied by substantial energy gain and this can be the driving force that facilitates ligand eliminations at the surface and vacancy filling in sub-surface layers. Densification thus accounts for some of the important characteristics of ALD, such as conformal growth.

Saturated surfaces: During the early stage of the metal pulse, due to the saturation of the surface by remaining fragments HfX, adsorption of further metal precursor stops. The presence of these fragments prevents further chemisorption of HfX_4, since this requires the creation of a strong dative bond between Hf and O. A separate effect is depletion of co-reagent (protons) at the surface as HX desorbs. Clearly, no further elimination of HX is possible once protons are exhausted. If the surface can store a higher population of co-reagent, then a higher growth rate is expected.[27] Next, during the H_2O pulse, Hf exchanges its remaining ligands with OH groups. The exchange occurs due to the decomposition of adsorbed H_2O molecules in clusters of HfX. Simultaneously, low coordinated oxygen atoms appear at the surface, which are reactive sites for the next metal pulse. With saturation of the surface by OH groups, H_2O molecules begin to appear. These molecules are loosely bonded to the surface and readily desorb, reducing the growth rate, especially at high

temperatures.

It can thus be seen that a wide variety of reactions can take place simultaneously on the surface during ALD. Competition between the elimination reactions and proton diffusion reactions at different ALD temperatures, and their influence on the conformality of the film, are interesting issues that we are currently investigating by incorporating these DFT data into kinetic Monte-Carlo modeling.

Acknowledgement

Financial support from the Science Foundation Ireland (SFI) strategic research cluster 'Functional Oxides and Related Materials for Electronics' (FORME), is gratefully acknowledged, www.tyndall.ie/forme. The authors also wish to acknowledge the SFI/HEA Irish Centre for High-End Computing (ICHEC) for the provision of computational facilities and support.

References

(1) Hurley, P. K. et al. *ECS Transactions* **2009**, *25*, 113–127.

(2) Puurunen, R. L. *Journal of Applied Physics* **2005**, *97*, 121301.

(3) Delabie, A.; Caymax, M.; Brijs, B.; Brunco, D.; Conard, T.; Sleeckx, E.; Ragnarsson, L.-A.; Van Elshocht, S.; De Gendt, S.; Heyns, M. *ECS Transactions* **2006**, *1*, 433–446.

(4) Hausmann, D. M.; Kim, E.; Becker, J.; Gordon, R. G. *Chemistry of Materials* **2002**, *14*, 4350–4358.

(5) Jeloaica, L.; Esteve, A.; Rouhani, M. D.; Esteve, D. *Applied Physics Letters* **2003**, *83*, 542–544.

(6) Widjaja, Y.; Musgrave, C. B. *The Journal of Chemical Physics* **2002**, *117*, 1931–1934.

(7) Mukhopadhyay, A. B.; Musgrave, C. B.; Sanz, J. F. *Journal of the American Chemical Society* **2008**, *130*, 11996–12006.

(8) Cho, M.; Park, H. B.; Park, J.; Lee, S. W.; Hwang, C. S.; Jang, G. H.; Jeong, J. *Applied Physics Letters* **2003**, *83*, 5503–5505.

(9) Olivier, S.; Ducere, J.-M.; Mastail, C.; Landa, G.; Esteve, A.; Rouhani, M. D. *Chemistry of Materials* **2008**, *20*, 1555–1560.

(10) Elliott, S. D. *Langmuir* **2010**, *26*, 9179–9182.

(11) Kohn, W.; Becke, A. D.; Parr, R. G. *The Journal of Physical Chemistry* **1996**, *100*, 12974–12980.

(12) Kresse, G.; Hafner, J. *Phys. Rev. B* **1993**, *47*, 558–561.

(13) Harris, J. *Phys. Rev. B* **1985**, *31*, 1770–1779.

(14) Perdew, J. P.; Burke, K.; Ernzerhof, M. *Phys. Rev. Lett.* **1996**, *77*, 3865–3868.

(15) Kresse, G.; Hafner, J. *Journal of Physics: Condensed Matter* **1994**, *6*, 8245.

(16) Payne, M. C.; Teter, M. P.; Allan, D. C.; Arias, T. A.; Joannopoulos, J. D. *Rev. Mod. Phys.* **1992**, *64*, 1045–1097.

(17) Elliott, S. D.; Greer, J. C. *J. Mater. Chem.* **2004**, *14*, 3246–3250.

(18) Zhao, X.; Vanderbilt, D. *Phys. Rev. B* **2002**, *65*, 233106.

(19) Aarik, J.; Aidla, A.; Kiisler, A.-A.; Uustare, T.; Sammelselg, V. *Thin Solid Films* **1999**, *340*, 110 – 116.

(20) Mukhopadhyay, A. B.; Sanz, J. F.; Musgrave, C. B. *Chemistry of Materials* **2006**, *18*, 3397–3403.

(21) Monkhorst, H. J.; Pack, J. D. *Phys. Rev. B* **1976**, *13*, 5188–5192.

(22) Kresse, G.; Hafner, J. *Phys. Rev. B* **1994**, *49*, 14251–14269.

(23) Ruggerone, P.; Ratsch, C.; Scheffler, M. Chapter 13 Density-functional theory of epitaxial growth of metals. In *Growth and Properties of Ultrathin Epitaxial Layers*; King, D., Woodruff, D., Eds.; Elsevier, 1997; Vol. 8, pp 490 – 544.

(24) Henkelman, G.; Uberuaga, B. P.; Jonsson, H. *The Journal of Chemical Physics* **2000**, *113*, 9901–9904.

(25) Henkelman, G.; Jonsson, H. *The Journal of Chemical Physics* **2000**, *113*, 9978–9985.

(26) Zydor, A.; Kessler, V. G.; Elliott, S. D. *Phys. Chem. Chem. Phys.* **2012**, *14*, 7954–7964.

(27) Weinreich, W.; Tauchnitz, T.; Polakowski, P.; Drescher, M.; Riedel, S.; Sundqvist, J.; Seidel, K.; Shirazi, M.; Elliott, S. D.; Ohsiek, S.; Erben, E.; Trui, B. *Journal of Vacuum Science & Technology A: Vacuum, Surfaces, and Films* **2013**, *31*, 01A123.

Graphical TOC Entry

